www.springer.com/41230
https://doi.org/10.1007/s41230-022-2033-y

An accelerated aging assisted by electric current in a Fe-Mn-Al-C low-density steel

Zhi-gang Wang, Chu-lun Shen, Jian-lei Zhang, *Chang-jiang Song, and Qi-jie Zhai

Center for Advanced Solidification Technology (CAST), School of Materials Science and Engineering, Shanghai University, Shanghai 200444, China

Abstract: An aging method assisted by electric current was applied to a Fe-18Mn-9Al-1C (wt.%) low-density steel. It improves the microstructure and therefore significantly increases both the yield strength and ductility of the steel. This current-assisted aging method can increase the yield strength by 178 MPa and elongation by 1.16 times in only 0.5 min at 450 °C. However, the yield strength is increased only 90 MPa by the traditional aging method (heat conduction) at 450 °C for 180 min, and the elongation is even decreased from 42.0% to 31.6%. The obvious improvement in yield strength by the current-assisted aging for a short time is resulted from the fact that the current-assisted aging promotes a rapid precipitation of nano-scale κ-carbides in γ-austenite by reducing the thermodynamic barrier and accelerating the atomic diffusion. This work demonstrates that this current-assisted aging method is significantly time saving and cost-effective for low-density steels, with potential for various industrial applications.

Keywords: low-density steel; current-assisted aging; κ-carbide

CLC numbers: TG142 **Document code:** A **Article ID:** 1672-6421(2022)05-395-08

1 Introduction

Owing to the demand for energy saving and consumption reduction, austenite-based Fe-Mn-Al-C steel with low-density and excellent mechanical properties has been attracting a lot of attention [1-5]. In this low-density steel, precipitation strengthening by nano-scale intragranular κ-carbides is an important method to increase the yield strength [6-10], but the ductility would be significantly reduced if coarse κ-carbides are formed at grain boundaries [11-13]. Therefore, the adjustment of κ-carbide precipitation plays an important role in obtaining excellent comprehensive mechanical properties of low-density steel.

Aging treatment in the temperature range of 450–650 °C has been proved to promote the precipitation of nano-scale κ-carbides and improve the strength of low-density steels without significant adverse effects on the plasticity [14]. However, in order to improve the strength of steels significantly, a long holding time is required for the traditional aging process (heat conduction), which leads to low production efficiency and high energy consumption. For example, it took 12 h to increase yield strength by 500 MPa at 450 °C in an austenite-based Fe-28Mn-9Al-1.8C low-density steel [12]. Therefore, it is necessary to find an efficient and low-energy-consumption aging method to improve the mechanical properties of low-density steel.

As an alternative to traditional aging, an aging method assisted by electric current, which rapidly heats the sample to target temperature and holds it for a short time, has attracted a lot of attention [15-18]. Wang et al. [19] revealed that the Cr-rich lamellae and Cr-rich precipitation with various shapes could be precipitated in a Cu-Cr-Zr alloy by direct current-assisted aging at a lower temperature than traditional aging, due to improvement of the diffusivity and mobility of vacancies. He et al. [20] found that the peak yield strength of 7B04 aluminum alloy could reach 655 MPa after direct current-assisted aging at 120 °C for 12 h, while for traditional aging treatment, it needed 24 h to reach the similar value of 632 MPa. This difference was attributed to the higher Zn-rich precipitation density of current-assisted aged samples in the Guinier-Preston II zones. Both the examples demonstrated that applying electric current in aging could promote precipitation of the Cr-rich and Zn-rich phases and improve microstructure at a lower temperature and in a shorter time compared with the

***Chang-jiang Song**

Ph.D., Professor. His research interests mainly focus on solidification theory and microstructure control, and fabrication of super performance metastable engineering materials through solidification process control. He has supervised over 20 projects and published more than 100 papers in international journals.

E-mail: riversong@shu.edu.cn; riversxiao@163.com

Received: 2022-03-02; Accepted: 2022-05-13

traditional aging. But few relevant studies on low-density steels have been reported.

In this work, the austenite-based Fe-18Mn-9Al-1C low-density steel was prepared by centrifugal casting. The aging assisted by electric current was then carried out, and its effect on microstructure and properties of the steel was investigated and compared with that by the traditional heat aging. The aging mechanism was also discussed.

2 Experimental procedure

The Fe-18Mn-9Al-1C (wt.%) steels were prepared by centrifugal casting under near-rapid solidification in an argon atmosphere. Firstly, pure iron (99.99%), pure manganese (99.9%), pure aluminum (99.9%) and high-purity graphite (99.8%) were melted in a cold-crucible levitation melting setup, and then an ingot was obtained. Then, the alloy ingot was re-melted by induction melting, and the molten metal was poured into a copper mold rotating at 600 rpm through a graphitic funnel and solidified in a few seconds (the calculated cooling rate was about 5×10^3 °C·s^{-1} [21]). Finally, a steel strip with the size of 60 mm×80 mm×2.5 mm was obtained. The schematic illustration of centrifugal casting equipment is shown in Fig. 1 [21].

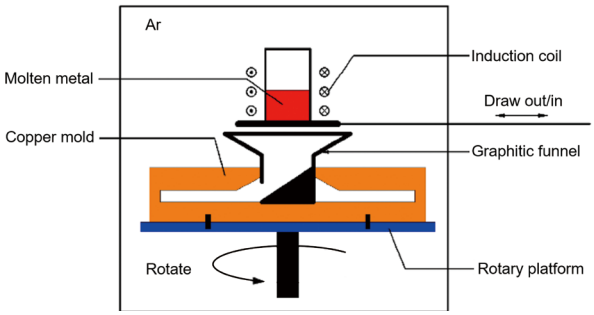

Fig. 1: Schematic illustration of centrifugal casting equipment [21]

Both the aging assisted by electric current (EA) and traditional method (TA) were carried out for the steel samples. Previous studies [22] have shown that aging at 450 °C contributes to the κ-carbide precipitation in γ-austenite, so the aging temperature was set to 450 °C. Figure 2(a) shows the schematic diagram of the two aging methods. When the low-density steel samples were aged by EA, both ends of the samples with a size of 53 mm×30 mm×1 mm were connected to the electrodes, as shown in Fig. 2(b). The sample was heated to 450 °C in 1 min and held for different times (0.5, 3, 6, 12, 18, 24 and 30 min), then, quick cooling was achieved by argon gas flow. The cooling rate was ~100 °C·s^{-1}. K-type thermocouples were directly welded on the sample surface to measure the temperature change. In the isothermal stage, the voltage was about 1 V, the current was around 35 A. The TA treatment was carried out in a resistance furnace and heated by heat conduction. The heating time of the TA method was 90 min and the aging time was 12 min, 60 min and 180 min; the cooling time in the furnace was about 4 h.

The composition of the studied steel was measured as Fe-18.13Mn-9.11Al-0.98C (wt.%), by using an Inductively Coupled Plasma Mass Spectrometry (ICP) and a CS2800 carbon-sulfur analyzer. Phase constitution was characterized by an X-ray diffraction (XRD, D/Max-2200, Cu target operated at 40 kV and 40 mA) with a scanning rate of 4°·min^{-1}. Microstructure was characterized by a scanning electron microscope (SEM, Phenom Pro). SEM samples were prepared by electrolytic polishing using the solutions of 10vol.% perchloric acid and 90vol.% alcohol. Transmission electron microscopy (TEM) was performed using a JEOL-2010F microscope operated at 200 kV. At least three tensile tests were carried out at room temperature using a MTS 44 machine to measure mechanical properties of each condition. The gauge size of the tensile samples was 20 mm×4 mm×1 mm, and the strain rate during tensile testing was 2.5×10^{-4} s^{-1}.

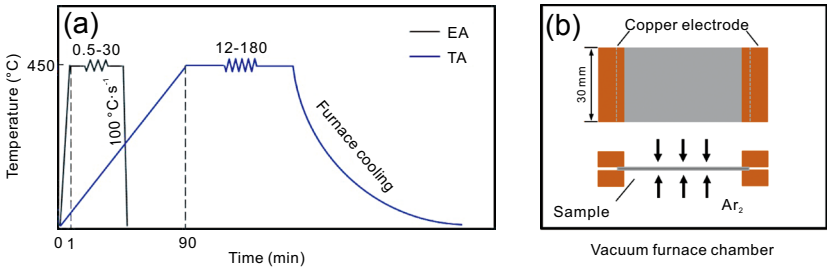

Fig. 2: Schematic diagram of electric current (EA) and traditional method (TA) processes (a), and the rapid aging equipment with electric current (b)

3 Results

3.1 Microstructure

Figure 3 shows the XRD patterns of the as-cast and aged samples. It can be seen that all the steel samples mainly consist of γ-austenite and δ-ferrite. With increasing the aging time, the intensities of all the diffracted peaks corresponding to δ-ferrite phase have no obvious change in both EA and TA cases, as shown in Fig. 3.

Figure 4 shows the SEM micrographs of as-cast and aged samples. Figure 4(a) shows that in the as-cast steel, short rod-shape δ-ferrite and irregular shape δ-ferrite distribute in γ-austenite matrix. After TA and EA treatment, the morphology of the low-density steels has no significant change, as shown in Figs. 4(b–f). However, after careful analysis on the end of δ-ferrite, as shown by the dotted line in Fig. 4(f), it can be found that the original sharp ends tend to be smooth after EA treatment. This phenomenon is related to the local Joule

heating effect of electric current [23, 24]. The average volume fraction of δ-ferrite was measured at ten different sites by using an image processing software (Image-Pro Plus, IPP), and the measured results are also shown in Fig. 4. After TA and EA treatment, the volume fraction of δ-ferrite in the samples has no clear change.

3.2 Mechanical properties

Figure 5 shows the mechanical properties of the as-cast and aged Fe-18Mn-9Al-1C steels. For the samples aged by EA method, the yield strength (YS) is increased by about 178 MPa after aging at 450 °C for 0.5 min. With extension of the aging time, the yield strength shows a plateau stage without obvious change, as shown in Fig. 5(c). When the aging time is extended to 30 min, the yield strength decreases significantly. The elongation firstly increases and then decreases with increasing the aging time, and reaches the maximum of 54.5% at 12 min, which is 1.3 times of the as-cast sample. Moreover, the ultimate tensile strength has a peak value at 0.5 min, then decreases with increasing the aging time, and changes little after 6 min. For the samples aged by TA method, the yield strength gradually increases with the extension of aging time, but only increases by about 90 MPa after aging at 450 °C for 180 min. The ultimate tensile strength reaches the maximum at 60 min and then decreases. The elongation increases slightly after aging for 12 min, and further increases to 44.7% when aging time is extended to 60 min, but decreases to 31.6% after aging for 180 min.

3.3 Precipitated phase

As mentioned above, the current-assisted aging can greatly increase strength and elongation of the low-density steels in a short time, while the microstructures of the samples aged with and without current assistance are almost the same (Figs. 3 and 4). The κ-carbide in γ-austenite plays a key role in the mechanical

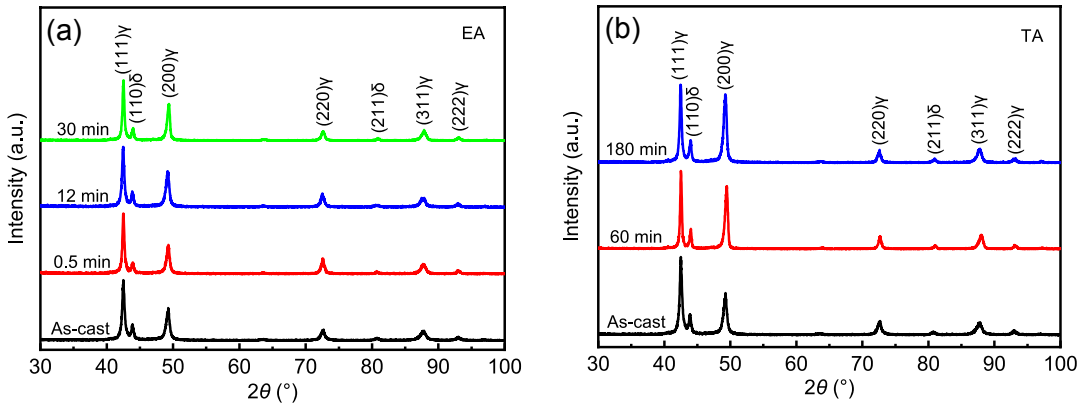

Fig. 3: X-ray diffraction patterns of the Fe-18Mn-9Al-1C low-density steels with different aging method and aging time: (a) EA; (b) TA

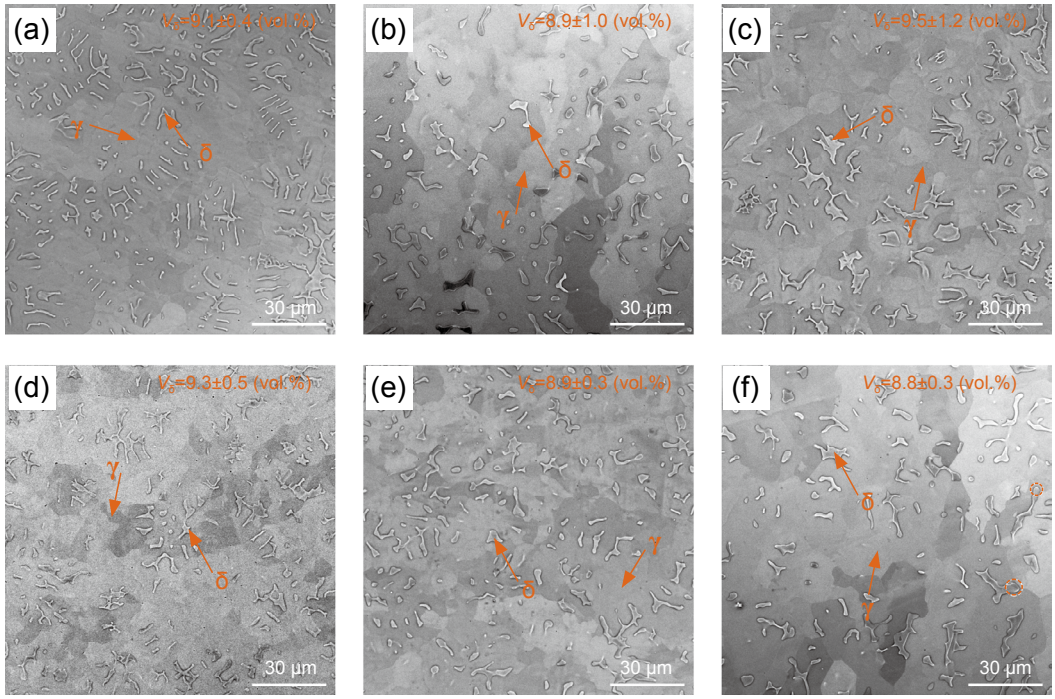

Fig. 4: SEM micrographs of the low-density steels before and after TA and EA treatment: (a) as-cast; (b) TA-60 min; (c) TA-180 min; (d) EA-0.5 min; (e) EA-12 min; (f) EA-30 min

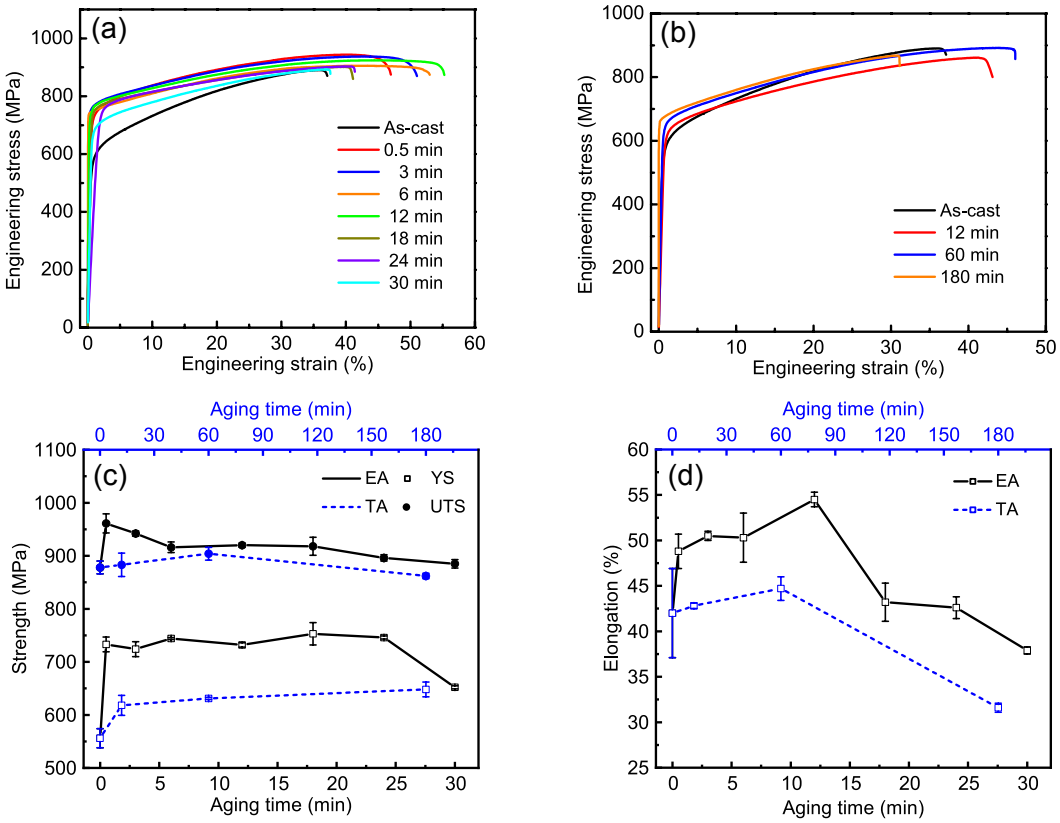

Fig. 5: Mechanical properties of low-density steels aged by two methods: (a) engineering stress-strain by EA; (b) engineering stress-strain by TA; (c) strength; (d) elongation

properties of low-density steel [25], so the precipitated particles in γ-austenite of the as-cast and aged steels were observed by TEM. Figure 6 shows the κ-carbides precipitates in γ-austenite of the as-cast and aged samples and Fig. 7 shows the statistical results of the κ-carbide average size and the number density. The average size of κ-carbides was obtained by measuring 100 κ-carbide particles using IPP software. The number density of κ-carbides was determined by counting the number of carbides in 100 nm^2. As shown in the selected area electron diffraction pattern taken from $[110]_{\gamma+\kappa}$ axis in Fig. 6, there are so many superlattice reflection spots belonging to κ-carbides, and the dark field images also show that there are many κ-carbides in the austenitic matrix. As shown in Fig. 7, for the samples aged by TA method, the average size of κ-carbides in γ-austenite changes little after aging for 60 min, while the number density increases from 1.07×10^{24} m^{-3} to 1.93×10^{24} m^{-3}. After aging for 180 min, the average size of κ-carbides is increased from 3.3 nm to 4.1 nm, but the number density slightly decreases. For the samples aged by EA method, the average size of κ-carbides in γ-austenite is increased from 3.3 nm to 4.6 nm and the number density is increased to 2.52×10^{24} m^{-3} after aging for 0.5 min. With the extension of aging time, the average size of κ-carbides tends to decreases, but the number density gradually increases. After EA treatment for 30 min, the average size of κ-carbides in the steel is decreased to 3.8 nm, and the number density is increased to 2.92×10^{24} m^{-3}. Compared with the TA method, a larger number of κ-carbides are precipitated in only 0.5 min by EA method.

4 Discussion

4.1 Mechanical properties of aged steels

The yield strength of the steels is increased by both aging methods, but the steel after the EA method has higher yield strength [Fig. 5(c)]. According to Fig. 7, the average size and number density of κ-carbides significantly increase after EA treatment for 0.5 min, which should be the main reason for the great improvement in yield strength. The smaller average size and number density of κ-carbides in the steels after TA treatment result in a lower strength.

The change of elongation is related to dislocation density, size and number density of κ-carbides particles [13, 26]. Generally, the decrease of dislocation density in steels before deformation is considered to improve the elongation, and more precipitations lead to the decrease of elongation.

Due to the rapid cooling rate during near-rapid solidification, the sample has a high thermal stress, which results in a great number of dislocations in the as-cast steel. Dislocation density can be estimated according to the Williamson Hall method and expressed as [27, 28]:

$$\rho=\frac{2\sqrt{3}\varepsilon}{db} \tag{1}$$

where b is the Burch vector, d is the grain diameter, and ε is the micro stress. ε is determined by the slope of the liner fit plot of $\beta\cos\theta$–$4\sin\theta$, where β is the half-width of the XRD

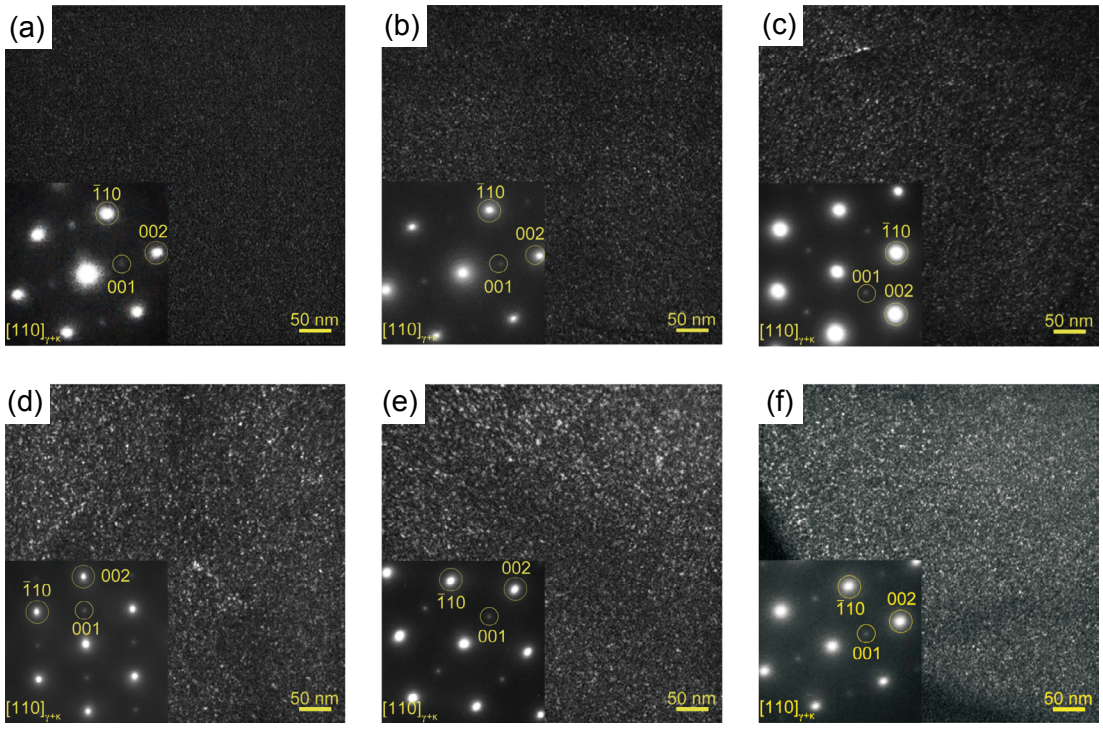

Fig. 6: TEM DF micrographs of κ-carbide in low-density steels: (a) as-cast; (b) TA-60 min; (c) TA-180 min; (d) EA-0.5 min; (e) EA-12 min; (f) EA-30 min

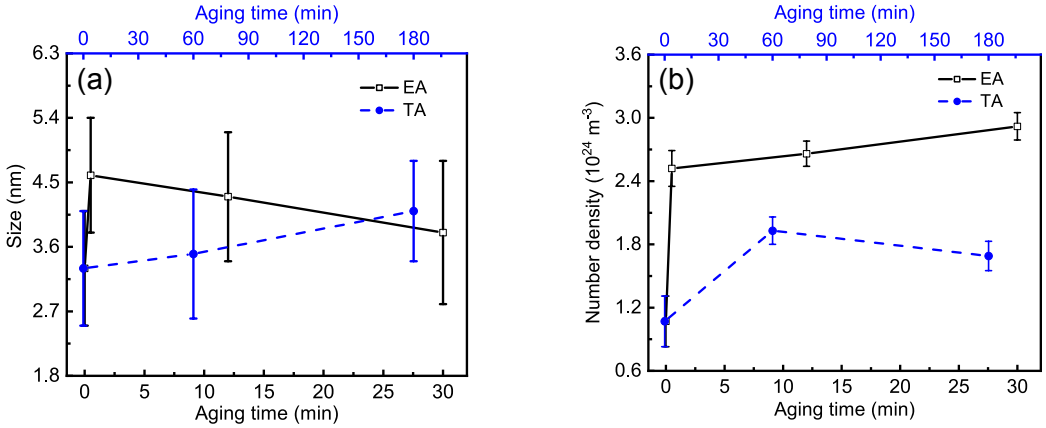

Fig. 7: Average size (a) and number density (b) of κ-carbides

diffraction peak for γ-austenite (111), (200), (220), θ is the Bragg angle of the X-ray diffraction peak. The calculation results of dislocation density are shown in Fig. 8, in which an obviously decrease of dislocation density occurs in the steels after EA treatment. This is the result of the drifting electrons exerting an extra pushing force on the dislocation during the aging with electric current [29], and this force can accelerate the dislocation annihilation [30-31]. The rapid decrease of dislocation density is beneficial to the increase of elongation.

According to Fig. 7, the κ-carbides in the steel after EA treatment are relatively larger and greater in number, which should not be conducive to plasticity. However, the EA treatment makes the κ-carbides at grain boundary finer compared with the κ-carbides in the steels after TA treatment, as shown in Fig. 9. The average size of κ-carbides at the grain boundary was measured by using IPP software. The average

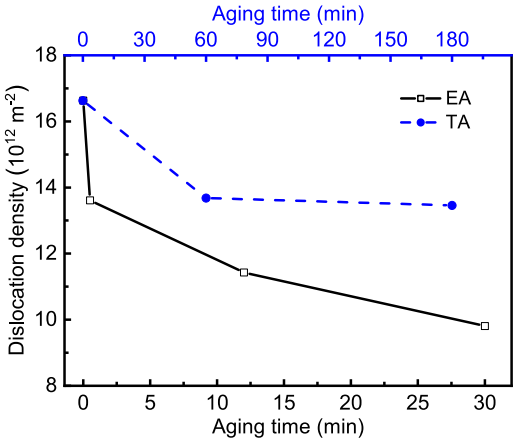

Fig. 8: Dislocation density in austenite of the steels after EA and TA

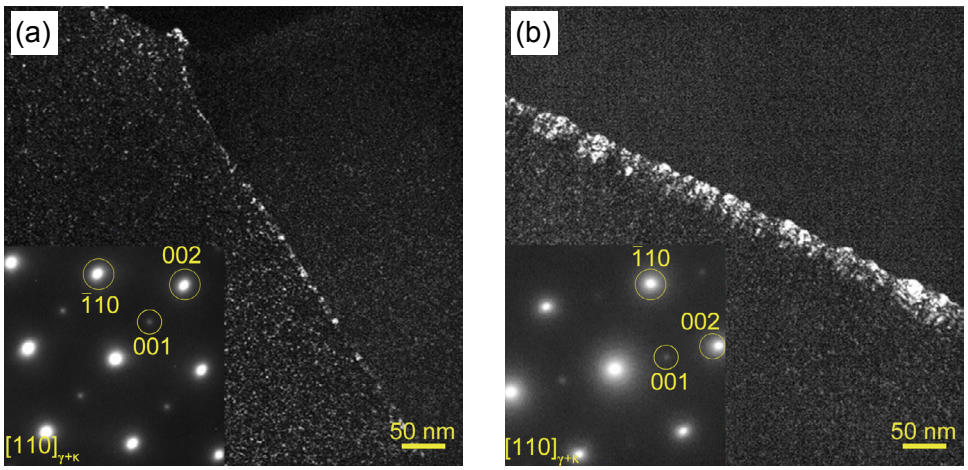

Fig. 9: TEM DF micrographs of γ-austenite at grain boundary in the steels: (a) EA-12 min; (b) TA-60 min

size of κ-carbides at the grain boundary in the steel after EA treatment for 12 min is only 4.8 nm, while that after TA treatment for 60 min is 8.3 nm. Smaller intergranular κ-carbide size after EA treatment makes the steel achieve better elongation.

Although dislocation reduces, the elongation significantly reduces after EA treatment for 30 min. One reason is due to the increase in the κ-carbide number within grains in steel. The other reason is that the high angle grain boundaries caused by current could also result in the decrease of elongation [32-34]. Waryoba et al. [32] found that the number of high angle grain boundaries in the Zircaloy-4 alloy was increased after electric current annealing at 135 °C for 10 min, which could effectively increase grain boundary strengthening but greatly decrease the elongation [35, 36]. Therefore, due to the rapid decrease of dislocation density in the steel by EA treatment, the elongation of the steel after EA treatment for a short time increases. When the aging time is prolonged, the more precipitation and high angle grain boundaries lead to the decrease of elongation.

4.2 Aging mechanism of electric current

As mentioned above, a shorter aging time with electric current can achieve higher yield strength and simultaneously better plasticity. Therefore, this aging method by electric current is a rapid and efficient aging method to improve the mechanical properties of low-density steel. Due to the aging temperature of the two aging methods being the same, the Joule heating alone is not enough to explain the above precipitation phenomenon by EA treatment. The enhancement of precipitation should be due to the change of activation free energy caused by electric current [16, 18]. When a current is applied to the material, the current increases the total free energy of the system. At this point, the nucleation rate I_e can be approximated as [31, 37]:

$$I_e = I_0\left(\frac{D}{\lambda^2}\right)\exp\left(-\frac{\Delta G_0 + \Delta G_{EC}}{kT}\right) \quad (2)$$

where I_0 is a constant related to kinetic factor, λ, D, k and T are jump distance, diffusion coefficient, Boltzmann constant and absolute temperature, respectively. ΔG_0 is the free energy to be required for nucleation without current, and ΔG_{EC} is the free energy associated with current. According to Eq. (2), when there is no current passing through the sample, $\Delta G_{EC}=0$, the free energy required for nucleation is ΔG_0. When there is current passing through the sample, the free energy required for nucleation becomes $\Delta G=\Delta G_0+\Delta G_{EC}$. The precipitation of κ-carbides improves the conductivity of γ-austenite matrix, $\Delta G_{EC}<0$ [38, 39], so $\Delta G<\Delta G_0$. The free energy required for κ-carbides nucleation is lower in EA samples, therefore, the nucleation rate of κ-carbides is increased.

Generally, the growth and coarsening of precipitates are controlled by atomic diffusion [40]. According to the theory of electromigration, fast-moving electrons can increase the diffusion rate of atoms when an electric current is applied [41]. The atomic diffusion flux J_e caused by the electric current effect can be expressed as [41, 42]:

$$J_e = C_i\frac{D_0}{kT}\exp\left(\frac{E_a}{kT}\right)Z^*e\rho j \quad (3)$$

where C_i is vacancy concentration, D_0 is pre-exponential diffusion factor, E_a is the activation energy for diffusion, k is Boltzmann constant, T is absolute temperature, Z^* is effective charges, e is charge, ρ is electric resistivity, and j is electric current density. In the thermal field, according to Fick's law, the atomic diffusion flux J_c caused by concentration gradient can be expressed as:

$$J_c = D_i\left(-\frac{\partial C_i}{\partial x}\right) \quad (4)$$

where D_i is diffusion coefficient, C_i is atomic volume concentration, $\frac{\partial C_i}{\partial x}$ is concentration gradient, and the '–' indicates that the diffusion direction is opposite to the concentration gradient. Combining diffusion law with electromigration theory, the total diffusion flux (J) of atoms under the coupling action of thermal field and electric field can be described as $J=J_e+J_c$. Therefore, when the current is applied to the sample, besides the concentration gradient, the nonthermal effect of the current will also affect the atomic diffusion at the same temperature. Compared with TA treatment, the atomic diffusion flux generated by the nonthermal effect of current causes the κ-carbides to grow rapidly after precipitation.

However, the size of κ-carbides tends to decrease beyond some aging time, which was also observed by Xu et al [43]. The reason is analyzed as follows: The precipitation of κ-carbides introduces a surrounding elastic strain field due to the lattice mismatch with the matrix [44]. This elastic stress can increase the resistivity of the conductor [45], which can lead to nonuniform distribution of current and a local intensifying current effect. Lu et al. [46] found that electric pulse could dissolve lamellar κ-carbides at a lower temperature. Therefore, it is possible that the precipitation and dissolution of κ-carbides coexist in the aging process assisted by electric current. In the steel with a short aging time by electric current, the precipitation of κ-carbides is dominant. From 0.5 min to 30 min, the dissolution of the growing κ-carbides frequently occurs, resulting in a decrease in the size of κ-carbides from 4.6 nm to 3.8 nm.

In short, under the coupling of thermal and nonthermal effects of electric current, rapid precipitation of nano-scale κ-carbides and decrease of dislocation density simultaneously increase aging strength and plasticity in a short time after EA treatment. With the precipitation and growth of κ-carbides, the distribution of the current becomes nonuniform, resulting in the enhancement of local thermal effect by current [16, 18]. The local thermal effect of current results in the dissolution of coarse κ-carbides and the reduction of κ-carbide size [47]. The size of κ-carbides tends to decrease, but the number increases further. Therefore, the average size of κ-carbides after EA treatment for 30 min is slightly smaller than that after TA treatment for 180 min. While the growth of κ-carbides is inhibited, dislocation density decreases rapidly, so that aging strength enters a platform period from 0.5 min to 24 min during EA treatment. At the same time, the decreased dislocation density causes plasticity to increase in the early stage of EA treatment, and elongation reaches its maximum at 12 min. But with the increase of the number of κ-carbides and the reduction rate of dislocation density slowing down, the plasticity gradually decreases [48-51].

5 Conclusions

In this work, an aging method assisted by electric current was investigated in a Fe-18Mn-9Al-1C (wt.%) low-density steel, and its microstructure and mechanical properties were compared with those of the traditional aging method. According to the experimental results, the following conclusions could be drawn:

(1) The electric current assisted aging treatment at 450 °C for 0.5 min can increase the strength of Fe-18Mn-9Al-1C low-density steel by 178 MPa and simultaneously, the elongation by 1.16 times. While, at the same aging temperature, the strength of the alloy only increases by 90 MPa by traditional aging treatment although for a long time of 180 min, and the elongation is decreased.

(2) A great number of κ-carbides precipitate from γ-austenite and the size and number density of the κ-carbides increase significantly after electric current assisted aging treatment at 450 °C for 0.5 min. With the extension of aging time, the size of κ-carbides decreases, but the number density increases. In addition, the number density of κ-carbides is much higher in the low-density steel after electric current assisted aging treatment for 0.5 min than that after traditional aging treatment for 180 min.

(3) The electric current assisted aging treatment increases the κ-carbide content by promoting atomic diffusion in austenite, reducing the thermodynamic barrier of κ-carbide, and accelerating the elimination of dislocations, which causes the low-density steel to show a better comprehensive performance.

Acknowledgements

This work was financially supported by the National MCF Energy R&D Program of China (No. 2018YFE0306102), the National Natural Science Foundation of China (No. 51974184), and the Joint Fund of Iron and Steel Research (No. U1660103).

References

[1] Zhang J L, Hu C H, Zhang Y H, et al. Microstructures, mechanical properties and deformation of near-rapidly solidified low-density Fe-20Mn-9Al-1.2C-*x*Cr steels. Materials & Design, 2020, 186: 108307.
[2] Zhang J L, Jiang Y S, Zheng W S, et al. Revisiting the formation mechanism of intragranular κ-carbide in austenite of a Fe-Mn-Al-Cr-C low-density steel. Scripta Materialia, 2021, 199: 113836.
[3] Liu Y X, Liu M X, Zhang J L, et al. Microstructure and mechanical properties of a Fe-28Mn-9Al-1.2C-(0, 3, 6, 9)Cr austenitic low-density steel. Materials Science & Engineering: A, 2021, 821: 141583.
[4] Chen Z, Liu M X, Zhang J K, et al. Effect of annealing treatment on microstructures and properties of austenite-based Fe-28Mn-9Al-0.8C lightweight steel with addition of Cu. China Foundry, 2021, 18(3): 207–216.
[5] Zhang J L, Hu C H, Liu Y X, et al. Precipitation strengthening of nano-scale TiC in a duplex low-density steel under near-rapid solidification. Journal of Iron & Steel Research International, 2021, 28(9): 1141–1148.
[6] Frommeyer G, Brüx U. Microstructures and mechanical properties of high-strength Fe-Mn-Al-C light-weight triplex steels. Steel Research International, 2006, 77(9–10): 627–633.
[7] Howell R A, Van Aken D C. A literature review of age hardening Fe-Mn-Al-C alloys. Iron & Steel Technology, 2009, 6(4): 193–212.
[8] Gutierrez-Urrutia I, Raabe D. High strength and ductile low density austenitic FeMnAlC steels: Simplex and alloys strengthened by nanoscale ordered carbides. Materials Science & Technology, 2014, 30(9): 1099–1104.
[9] Suh D W, Park S J, Lee T H, et al. Influence of Al on the microstructural evolution and mechanical behavior of low-carbon, manganese transformation-induced-plasticity steel. Metallurgical & Materials Transactions A, 2009, 41(2): 397–408.
[10] Zhang L F, Song R, Zhao C, et al. Evolution of the microstructure and mechanical properties of an austenite-ferrite Fe-Mn-Al-C steel. Materials Science & Engineering: A, 2015, 643: 183–193.
[11] Zhang J L, Raabe D, Tasan C C. Designing duplex, ultrafine-grained Fe-Mn-Al-C steels by tuning phase transformation and recrystallization kinetics. Acta Materialia, 2017, 141: 374–387.
[12] Chang K M, Chao C G, Liu T F. Excellent combination of strength and ductility in an Fe-9Al-28Mn-1.8C alloy. Scripta Materialia, 2010, 63(2): 162–165.
[13] Lin C L, Chao C G, Bor H Y, et al. Relationship between microstructures and tensile properties of an Fe-30Mn-8.5Al-2.0C alloy. Materials Transactions, 2010, 51(6): 1084–1088.

[14] Jeong S, Park G, Kim B, et al. Precipitation behavior and its effect on mechanical properties in weld heat-affected zone in age hardened femnalc lightweight steels. Materials Science & Engineering: A, 2019, 742: 61–68.
[15] Sprecher A F, Mannan S L, Conrad H, et al. Overview No. 49: On the mechanisms for the electroplastic effect in metals. Acta Metallurgica, 1986, 34(7): 1145–1162.
[16] Xu X F, Zhao Y G, Ma B D, et al. Electropulsing induced evolution of grain-boundary precipitates without loss of strength in the 7075 Al alloy. Materials Characterization, 2015, 105: 90–94.
[17] Yang S Z, Li N, Wen Y H, et al. Effects of ageing with electric pulse treatment on shape memory effect and precipitation of $Cr_{23}C_6$ carbide in a pre-deformed Fe-Mn-Si-Cr-Ni-C alloy. Rare Metal Materials & Engineering, 2013, 42(2): 238–242.
[18] Xu X F, Zhao Y G, Ma B D, et al. Rapid precipitation of T-phase in the 2024 aluminum alloy via cyclic electropulsing treatment. Journal of Alloys & Compounds, 2014, 610: 506–510.
[19] Wang Z Q, Zhong Y B, Lei Z S, et al. Microstructure and electrical conductivity of Cu-Cr-Zr alloy aged with DC electric current. Journal of Alloys & Compounds, 2009, 471(1): 172–175.
[20] He L Z, Wei M X, Ning Q B, et al. Effects of applying direct current on microstructures and properties of 7B04 aluminum alloy during solid solution and artificial ageing. Rare Metal Materials & Engineering, 2020, 49(6): 1957–1962.
[21] He W, Wang B L, Yang Y, et al. Microstructure and mechanical behavior of a low-density Fe-12Mn-9Al-1.2C steel prepared using centrifugal casting under near-rapid solidification. Journal of Iron & Steel Research International, 2018, 25(8): 830–838.
[22] Chen S P, Rana R, Haldar A, et al. Current state of Fe-Mn-Al-C low density steels. Progress in Materials Science, 2017, 89: 345–391.
[23] Qin R S, Samuel E I, Bhowmik A. Electropulse-induced cementite nanoparticle formation in deformed pearlitic steels. Journal of Materials Science, 2011, 46(9): 2838–2842.
[24] Xu X F, Zhao Y G, Ma B D, et al. Rapid precipitation of T-phase in the 2024 aluminum alloy via cyclic electropulsing treatment. Journal of Alloys & Compounds, 2014, 610: 506–510.
[25] Lu W J, Zhang X F, Qin R S. κ-carbide hardening in a low-density high-Al high-Mn multiphase steel. Materials Letters, 2015, 138: 96–99.
[26] Lin Y J, Zhang Y G, Xiong B Q, et al. Achieving high tensile elongation in an ultra-fine grained Al alloy via low dislocation density. Materials Letters, 2012, 82: 233–236.
[27] Williamson G K, Smallman R E. Dislocation densities in some annealed and cold-worked metals from measurements on the D-ray Debye-Scherrer spectrum. Philosophical Magazine, 1956, 1(1): 34–46.
[28] Zhao Y H, Liao X Z, Jin Z, et al. Microstructures and mechanical properties of ultrafine grained 7075 Al alloy processed by ECAP and their evolutions during annealing. Acta Materialia, 2004, 52(15): 4589–4599.
[29] Li X Q, Turner J, Bustillo K, et al. In situ transmission electron microscopy investigation of electroplasticity in single crystal nickel. Acta Materialia, 2022, 223: 117461.
[30] Conrad H, Karam N, Mannan S. Effect of electric current pulses on the recrystallization of copper. Scripta Metallurgica, 1983, 17(3): 411–416.
[31] Rahnama A, Qin R S. Effect of electric current pulses on the microstructure and niobium carbide precipitates in a ferritic-pearlitic steel at an elevated temperature. Journal of Materials Research, 2015, 30(20): 3049–3055.
[32] Waryoba D, Islam Z, Wang B M, et al. Recrystallization mechanisms of Zircaloy-4 alloy annealed by electric current. Journal of Alloys and Compounds, 2020, 820: 153409.
[33] Jiang Y, Guan L, Tang G, et al. Influence of electropulsing treatment on microstructure and mechanical properties of cold-rolled Mg-9Al-1Zn alloy strip. Materials Science & Engineering: A, 2011, 528(16–17): 5627–5635.
[34] Li C, Tan H, Wu W M, et al. Effect of electropulsing treatment on microstructure and tensile fracture behavior of nanocrystalline Ni foil. Materials Science & Engineering: A, 2016, 657: 347–352.
[35] Canadinc D, Biyikli E, Niendorf T, et al. Experimental and numerical investigation of the role of grain boundary misorientation angle on the dislocation-grain boundary interactions. Advanced Engineering Materials, 2011, 13(4): 281–287.
[36] Niendorf T, Dadda J, Canadinc D, et al. Monitoring the fatigue-induced damage evolution in ultrafine-grained interstitial-free steel utilizing digital image correlation. Materials Science & Engineering: A, 2009, 517(1): 225–234.
[37] Qin R S, Zhou B L. Exploration on the fabrication of bulk nanocrystalline materials by direct-nanocrystallizing method II: Theoretical calculation of grain size of metals sondified under electropulsing. Chinese Journal of Materials Research, 1997, 11(1): 69–72.
[38] Wang X L, Guo J D, Wang Y M, et al. Segregation of lead in Cu-Zn alloy under electric current pulses. Applied Physics Letters, 2006, 89(6): 276–217.
[39] Jiang Y, Tang G, Shek C, et al. On the thermodynamics and kinetics of electropulsing induced dissolution of β-$Mg_{17}Al_{12}$ phase in an aged Mg-9Al-1Zn alloy. Acta Materialia, 2009, 57(16): 4797–4808.
[40] Jiang S H, Wang H, Wu Y, et al. Ultrastrong steel via minimal lattice misfit and high-density nanoprecipitation. Nature, 2017, 544: 460–464.
[41] Pierce D G, Brusius P G. Electromigration: A review. Microelectronics Reliability, 1997, 37(7): 1053–1072.
[42] Hao J Q, Zhang H X, Zhang X F, et al. Accelerated carbon atoms diffusion in bearing steel using electropulsing to reduce spheroidization processing time and improve microstructure uniformity. Steel Research International, 2020, 91(7): 2000041.
[43] Xu H, Liu M, Wang Y P, et al. Refined microstructure and dispersed precipitates in a gradient rolled AZ91 alloy under pulsed current. Materialia, 2021, 20: 101245.
[44] Yao M J. κ-carbide in a high-Mn light-weight steel: Precipitation, off-stoichiometry and deformation. Doctoral Dissertation: Aachen: Rheinisch-Westfälische Technische Hochschule, 2017: 98–106.
[45] Kalashnikov I S, Acselrad O, Shalkevich A, et al. Heat treatment and thermal stability of femnalc alloys. Journal of Materials Processing Technology, 2003, 136(1–3): 72–79.
[46] Lu W J, Qin R S. Influence of κ-carbide interface structure on the formability of lightweight steels. Materials & Design, 2016, 104: 211–216.
[47] Qin R S, Lu W J, Zhang X F, et al. Stability of precipitates under electropulsing in 316L stainless steel. Materials Science & Technology, 2015, 31(13): 1530–1535.
[48] Chen S P, Rana R, Haldar A, et al. Current state of Fe-Mn-Al-C low density steels. Progress in Materials Science, 2017, 89: 345–391.
[49] Hu T, Ma K, Topping T D, et al. Improving the tensile ductility and uniform elongation of high-strength ultrafine-grained Al alloys by lowering the grain boundary misorientation angle. Scripta Materialia, 2014, 78–79: 25–28.
[50] Xu W, Xin Y C, Zhang B, et al. Stress corrosion cracking resistant nanostructured Al-Mg alloy with low angle grain boundaries. Acta Materialia, 2022, 225: 117607.
[51] Chen X, Li R, Li B, et al. Achieving ultra-high ductility and fracture toughness in molybdenum via Mo_2TiC_2 MXene addition. Materials Science & Engineering: A, 2021, 818: 141422.